This is a repository copy of *Symmetry-reduced dynamic mode decomposition of near-wall turbulence*.

White Rose Research Online URL for this paper:
https://eprints.whiterose.ac.uk/183681/

Version: Submitted Version

Article:

Marensi, E. orcid.org/0000-0001-7173-4923, Yalnız, G., Hof, B. et al. (1 more author) (Submitted: 2021) Symmetry-reduced dynamic mode decomposition of near-wall turbulence. arXiv. (Submitted)

Symmetry-reduced Dynamic Mode Decomposition of Near-wall Turbulence

E. Marensi, G. Yalnız, B. Hof and N. B. Budanur†

IST Austria, Am Campus 1, 3400 Klosterneuburg Austria

Data-driven dimensionality reduction methods such as proper orthogonal decomposition (POD) and dynamic mode decomposition (DMD) have proven to be useful for exploring complex phenomena within fluid dynamics and beyond. A well-known challenge for these techniques is posed by the continuous symmetries, e.g. translations and rotations, of the system under consideration as drifts in the data dominate the modal expansions without providing an insight into the dynamics of the problem. In the present study, we address this issue for the pressure-driven flow in a rectangular channel by formulating a continuous symmetry reduction method that eliminates the translations simultaneously in the streamwise and spanwise directions. As an application, we consider turbulence in a minimal flow unit at a Reynolds number (based on the centerline velocity and half-channel height) $Re = 2000$ and compute the symmetry-reduced dynamic mode decomposition (SRDMD) of sliding data windows of varying durations. SRDMD of channel flow reveals episodes of turbulent time evolution that can be approximated by a low-dimensional linear expansion.

1. Introduction

Turbulence is a strongly nonlinear phenomenon exhibiting chaotic spatio-temporal behaviour at many scales. Despite its complexity, a certain degree of coherence is observed and has been studied for many years with the goal of describing dynamics of turbulent flows in terms of few *coherent structures* (Jiménez 2018*a*). In the context of wall-bounded flows, a considerable amount of research (see e.g. Hamilton *et al.* 1995; Waleffe 1997; Jiménez & Pinelli 1999; Schoppa & Hussain 2002) is devoted to understanding the turbulence-sustaining mechanisms in terms of *quasi-streamwise vortices* and *streaks*. The former term refers to coherent regions of vortically moving fluid transverse to the flow direction and the latter describes an elongated high- or low-speed modulation of the base flow. Despite the abundant numerical and experimental evidence supporting the importance of streaks in wall turbulence and the intuitive physical picture provided by their interactions with vortices, the definition of a streak is based on experimental observations and, thus, inherently subjective (Jiménez 2018*b*). Consequently, one does not know how much is lost by neglecting the rest of the fluctuations in turbulent flow.

A complementary, yet mathematically exact, approach to low-dimensionality in turbulence is provided by the so-termed (Waleffe 2001) *exact coherent structures* (ECS), which are unstable time-invariant (self-sustaining) solutions of the Navier–Stokes equations such as equilibria, travelling waves and periodic orbits. These correspond to compact low-dimensional objects in the infinite-dimensional *state space* of all possible flow fields and influence the dynamics in their vicinity via their stable and unstable manifolds (Gibson *et al.* 2008; van Veen & Kawahara 2011; Budanur *et al.* 2017, 2019; Budanur & Hof 2017, 2018; Suri *et al.* 2017). In other words, together with their stable and unstable manifolds, ECS provide the intrinsic coordinates that can transiently approximate turbulence. Despite the relevance of ECS being fully established for transitional and low-Reynolds-number turbulent

† Email address for correspondence: burak.budanur@ist.ac.at

flows (see extensive reviews by Kerswell 2005; Eckhardt *et al.* 2008; Kawahara *et al.* 2012), a main challenge of the past twenty years has been to find more and more complex solutions that can capture the flow dynamics at higher Reynolds numbers and in larger domains.

The current availability of large data sets, both from experiments and simulations, and ongoing developments of data-driven modelling tools offer new avenues for tackling the problem of identifying low-dimensional behaviour underlying complex fluid flows. Indeed, high-dimensional data can be fed into data-driven decomposition techniques to gain useful information about the underlying physical processes (Rowley & Dawson 2017). Amongst these methods, dynamic mode decomposition (DMD) (Schmid & Sesterhenn 2008; Schmid 2010) has been successfully applied to many complex fluid systems (for a comprehensive list see Rowley & Dawson 2017, table 3) with the aim of extracting dynamically important flow features from time-resolved data. DMD generates a hierarchy of flow fields (DMD modes) and the associated eigenvalues (DMD eigenvalues) that can be used to approximate the input data by a linear expansion. Finding a linear modal expansion to describe strongly nonlinear chaotic fluid dynamics might at first sound like a hopeless endeavour. However, such an approximation can be found for a finite time, similar, in spirit, to using a nonlinear invariant solution and its stable/unstable manifolds to approximate turbulent time evolution in its neighbourhood. One way of rationalizing this is through the interpretation of DMD modes as the eigenmodes of the best-fit linear system for the given data set (Kutz *et al.* 2016). Another reasoning follows from the correspondence between DMD and Koopman mode decomposition (Rowley *et al.* 2009), which, under certain assumptions, states that DMD can be interpreted as a finite-dimensional approximation to the spectrum of the linear Koopman operator (Koopman 1931; Mezić 2005) that acts on the observables associated with the dynamical system under consideration.

In this paper, we present a dynamic mode decomposition of the near-wall turbulence in the direct numerical simulation (DNS) of channel flow. The key technical advancement here is the preprocessing of data by symmetry reduction to eliminate the degeneracies due to streamwise and spanwise translations, which resolves the well-known shortcomings (Kutz *et al.* 2016; Sesterhenn & Shahirpour 2019) of DMD in systems with continuous symmetries. In such systems, the drifts in the continuous symmetry directions artificially increase the dimensionality of embeddings that can reliably capture the dynamics (Rowley & Marsden 2000; Mendible *et al.* 2020). Furthermore, in spatiotemporal systems with a continuous flux, such as the channel flow considered here, the drifting motion completely dominates the DMD spectra, obscuring the physically-important dynamics of the system under study. Through examples in the following, we demonstrate that the *symmetry-reduced dynamic mode decomposition* (SRDMD) of the channel flow resolves the aforementioned issues and reveals episodes of turbulence that can be reliably described by a low-dimensional linear expansion. The paper is organised as follows. In §2 and §3 we introduce channel flow with its symmetries and formulate a symmetry reduction method for this configuration. The DMD algorithm is summarised in §4 and then applied to the symmetry-reduced DNS data in §5. The necessity of symmetry reduction is demonstrated in §6 and concluding remarks are drawn in §7.

2. Channel flow, symmetries, and the numerical setup

We consider the pressure-driven fluid flow between two parallel plates in a computational domain $(x, y, z) \in [0, L_x] \times [-h, h] \times [0, L_z]$, where x, y, z are the streamwise, wall-normal and spanwise directions, respectively. We take the base-fluctuation decomposition $\boldsymbol{u}_{tot} = \boldsymbol{U} + \boldsymbol{u}$ where $\boldsymbol{U} = U_c(1 - y^2)\hat{\boldsymbol{x}}$ is the parabolic laminar flow and U_c is the centerline velocity. The fluctuating velocity field $\boldsymbol{u} = u\hat{\boldsymbol{x}} + v\hat{\boldsymbol{y}} + w\hat{\boldsymbol{z}}$ has zero net flux and satisfies

the incompressibility condition $\nabla \cdot \boldsymbol{u} = 0$. The boundary conditions are *no slip* on the walls, i.e. $\boldsymbol{u}(x, y = \pm h, z) = \boldsymbol{0}$, and periodic in the extended directions, i.e. $\boldsymbol{u}(x, y, z) = \boldsymbol{u}(x + L_x, y, z) = \boldsymbol{u}(x, y, z + L_z)$. We present our results to follow in the nondimensional units where $h = U_c = 1$ and define the Reynolds number $Re := \frac{U_c h}{\nu}$. Pressure-driven channel flow is equivariant under the translations

$$g(\delta x, \delta z)[u, v, w](x, y, z) = [u, v, w](x - \delta x, y, z - \delta z), \tag{2.1}$$

where $\delta x \in [0, L_x]$ and $\delta z \in [0, L_z)$, and the reflections

$$\sigma_y[u, v, w](x, y, z) = [u, -v, w](x, -y, z), \tag{2.2}$$

$$\sigma_z[u, v, w](x, y, z) = [u, v, -w](x, y, -z). \tag{2.3}$$

In our applications, we consider turbulent channel flow at Reynolds number $Re = 2000$ in a minimal flow unit (Jiménez & Moin 1991) of dimensions $L_z = 2\pi/5$ and $L_x = 2\pi/2.2$. We restrict our attention to turbulence near one wall by imposing σ_y-invariance (symmetry with respect to midplane) on the velocity fields. We note that imposing this symmetry does not alter the wall friction, nor does it restrict the continuous symmetries of the channel flow. Direct numerical simulations are carried out using the `Channelflow2.0` solver (Gibson *et al.* 2020) with grid resolution $N_x \times N_y \times N_z = 64 \times 97 \times 48$ which ensures a drop of at least 4 orders of magnitude in the spectra. The time step is dynamically adjusted so that the Courant–Friedrichs–Lewy number (*CFL*) satisfies $0.15 \leqslant CFL < 0.3$. The friction Reynolds number is $Re_\tau \approx 100$ and the minimal channel dimensions, expressed in wall units (Pope 2000), are $L_x^+ \approx 280$ and $L_z^+ \approx 120$.

3. Continuous symmetry reduction

The equivariance of channel flow under the translations (2.1) implies that if $\boldsymbol{u}(t)$ is a solution, so is $g(\delta x, \delta z)\boldsymbol{u}(t)$. In other words, each solution has infinitely many symmetry copies that can be obtained by translations in the streamwise and spanwise directions. Sirovich (1987*a*) showed that if such symmetry copies are included in the data set, its proper orthogonal decomposition (POD) results in POD modes that align with Fourier modes in the symmetry directions and thus carry no information about the physics of the system. As a remedy, Rowley & Marsden (2000) suggested reducing the symmetry degree of freedom prior to POD of the data obtained from a system with translation symmetry. Their method relied on an experimentally-chosen template to which the simulation data is matched. As noted by the authors themselves, such a symmetry reduction method has a finite domain of applicability, the boundary of which is set by the singularity of the so-called reconstruction equation. In the following, we take a similar approach and formulate a symmetry reduction method for preprocessing channel flow data prior to its DMD. Differently from Rowley & Marsden (2000), our method yields a symmetry reduction for all dynamics of interest.

Budanur *et al.* (2015*b*) showed that a polar coordinate transformation in the Fourier-space of a spatially extended system can be interpreted as a *slice*, that is, a codimension-1 manifold in the state space of the system where each set of translation-equivalent states is represented by its unique intersection with this manifold. On applications to the Kuramoto–Sivashinsky system, Budanur *et al.* (2015*b*) demonstrated that such a *first Fourier mode slice* can be used to reduce the translation symmetry of the flow for all dynamics of interest. Later, the method was successfully adapted to two-dimensional Kolmogorov (Farazmand 2016; Hiruta & Toh 2017) and three-dimensional pipe (Willis *et al.* 2016; Budanur & Hof 2017, 2018) flows; see Budanur *et al.* (2015*a*) for a pedagogical introduction. In the following, we present a straightforward adaptation of this method to channel flow. We begin by defining the slice

templates

$$\hat{\boldsymbol{u}}'_x \coloneqq f(y)\cos(2\pi x/L_x)\hat{\boldsymbol{x}} \quad \text{and} \quad \hat{\boldsymbol{u}}'_z \coloneqq f(y)\cos(2\pi z/L_z)\hat{\boldsymbol{x}}, \tag{3.1}$$

where $f(y)$ is a to-be-specified function of the wall-normal coordinate only. Let $\boldsymbol{u}$ be a solution of channel flow and the set $\mathcal{M}^x_{\boldsymbol{u}} = \{g(\delta x, 0)\boldsymbol{u} \mid \delta x \in [0, L_x]\}$ be formed by $\boldsymbol{u}$ and its streamwise-translation copies. The key idea behind the first Fourier mode slice is the observation that any non-zero projection of $\mathcal{M}^x_{\boldsymbol{u}}$ onto the plane spanned by $\hat{\boldsymbol{u}}'_x$ and its quarter-domain shift $g(L_x/4, 0)\hat{\boldsymbol{u}}'_x = f(y)\sin(2\pi x/L_x)\hat{\boldsymbol{x}}$ is of circular shape. Thus, a transformation that fixes the polar angle $\hat{\phi}_x \coloneqq \arg(\langle \boldsymbol{u}, \hat{\boldsymbol{u}}'_x\rangle + i\langle \boldsymbol{u}, g(L_x/4, 0)\hat{\boldsymbol{u}}'_x\rangle)$ where $\langle , \rangle$ denotes L_2 inner product, can be used to reduce the translation symmetry. Following analogous observations, we define $\hat{\phi}_z \coloneqq \arg(\langle \boldsymbol{u}, \hat{\boldsymbol{u}}'_z\rangle + i\langle \boldsymbol{u}, g(0, L_z/4)\hat{\boldsymbol{u}}'_z\rangle)$ and the symmetry-reducing transformations

$$S_x(\boldsymbol{u}) \coloneqq g\left(-(\hat{\phi}_x/2\pi)L_x, 0\right)\boldsymbol{u} \quad \text{and} \quad S_z(\boldsymbol{u}) \coloneqq g\left(0, -(\hat{\phi}_z/2\pi)L_z\right)\boldsymbol{u}. \tag{3.2}$$

Noting that the slice templates $\hat{\boldsymbol{u}}'_x(x, y)$ and $\hat{\boldsymbol{u}}'_z(y, z)$ in (3.1) do not depend on the z and x coordinates respectively and the translations in x and z directions commute, we reduce the streamwise and spanwise translations simultaneously by simply applying the transformations (3.2) consecutively as $\hat{\boldsymbol{u}} = S(\boldsymbol{u}) = S_z(S_x(\boldsymbol{u}))$.

Until now, we left the wall-normal dependence of the template functions (3.1) unspecified. To clarify this final point, we shall first give a geometric interpretation of our symmetry reduction. Since the symmetry reduction eliminates two continuous translation degrees of freedom, the symmetry-reduced velocity fields $\hat{\boldsymbol{u}}(t)$ are confined to a submanifold in the state space with two dimensions less than that accommodating the original velocity fields $\boldsymbol{u}(t)$. This information, however, is not lost and can be recovered as long as one keeps track of the slice phases $\hat{\phi}_x(t)$ and $\hat{\phi}_z(t)$. Rowley & Marsden (2000) showed that these phases can also be obtained by integrating the reconstruction equations

$$\dot{\hat{\phi}}_x(t) = \left(\frac{2\pi}{L_x}\right)\frac{\langle \partial_x\hat{\boldsymbol{u}}'_x, \partial_t\boldsymbol{u}|_{\boldsymbol{u}=\hat{\boldsymbol{u}}(t)}\rangle}{\langle \partial_x\hat{\boldsymbol{u}}'_x, \partial_x\hat{\boldsymbol{u}}(t)\rangle} \quad \text{and} \quad \dot{\hat{\phi}}_z(t) = \left(\frac{2\pi}{L_z}\right)\frac{\langle \partial_z\hat{\boldsymbol{u}}'_z, \partial_t\boldsymbol{u}|_{\boldsymbol{u}=\hat{\boldsymbol{u}}(t)}\rangle}{\langle \partial_z\hat{\boldsymbol{u}}'_z, \partial_z\hat{\boldsymbol{u}}(t)\rangle}. \tag{3.3}$$

Note that the phase velocities (3.3) diverge if the denominators of the reconstruction equations vanish, at which point our symmetry reduction method would suffer a discontinuity. With this in mind, we determine $f(y)$ in (3.1) such that the denominators of the reconstruction equations (3.3) never vanish. After some experimentation, we set $f(y) = 2.5T_2 - 1.25T_4 - 1.25T_6$, where T_i are the Chebyshev polynomials of the first kind. Fig. 1 shows the time series of phase velocities (3.3) for the turbulent channel flow states sampled using a time step $\delta t = 0.1$. The insets illustrate that apparent spikes in the time-series can be resolved by a higher temporal resolution. Supplementary Movie 1 shows a segment from this simulation where the original flow states are shown next to their symmetry-reduced counterparts.

4. Symmetry-reduced dynamic mode decomposition

Let $\xi(t)$ be the n-dimensional symmetry-reduced state vector corresponding to the fluid state at time t, $\Phi^t(\xi)$ be the finite-time flow induced by the DNS and symmetry reduction, and ξ_k ($k = 0, \ldots, m$) be snapshots of states that are separated in time by δt, i.e. $\xi_{k+1} = \Phi^{\delta t}(\xi_k)$. Defining the $n \times m$ ($n \gg m$) data matrices $\Xi \coloneqq [\xi_0, \xi_1, \ldots, \xi_{m-1}]$ and $\Xi' \coloneqq [\xi_1, \xi_2, \ldots, \xi_m]$, we consider the linear approximation $\Xi' \approx A\Xi$, where A is an $n \times n$ matrix. The best fit (in L_2 sense) to this approximation is given by $A = \Xi'\Xi^\dagger$, where $\dagger$ denotes the Moore–Penrose pseudoinverse. We adopt the standard DMD algorithm (Tu *et al.* 2014; Kutz *et al.* 2016), which approximates eigenvalues and eigenvectors of A without explicitly computing it as follows. Let $\Xi \approx U\Sigma V^*$ denote the rank-r ($r < m$) singular value decomposition (SVD) approximation
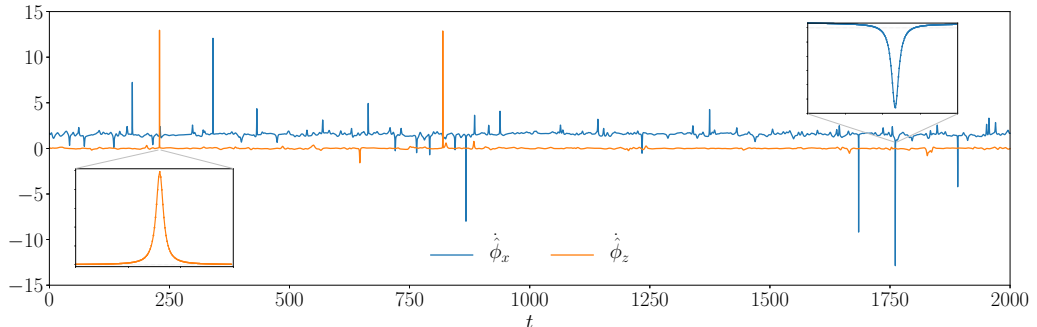
Figure 1: Time series of the slice phase velocities (finite-difference approximations to 3.3) for turbulent channel flow states sampled with time step $\delta t = 0.1$. Insets: zoom-ins to intervals with fast phase oscillations using $\delta t = 0.01$.

of Ξ, where $U \in \mathbb{C}^{n \times r}$, $\Sigma \in \mathbb{C}^{r \times r}$, $V \in \mathbb{C}^{m \times r}$ and * indicates the Hermitian transpose. Noting that the columns of U are the POD modes, we can rewrite the best-fit linear operator and its $r \times r$ projection onto the POD space as $A = \Xi' V \Sigma^{-1} U^*$ and $\tilde{A} = U^* A U = U^* \Xi' V \Sigma^{-1}$, respectively. Finally, we compute eigenvalues Λ_j and eigenvectors $\tilde{\psi}_j$ of $\tilde{A}$, from which we obtain the SRDMD modes as $\psi_j = \Xi' V \Sigma^{-1} \tilde{\psi}_j$. Defining $\lambda_j := \log(\Lambda_j)/\delta t$, we can now write the SRDMD-approximation of the time-evolution as

$$\tilde{\xi}(t) = \sum_{j=0}^{N_d-1} c_j \psi_j e^{\lambda_j t} \approx \xi(t),$$ (4.1)

where c_j are the SRDMD coefficients and $N_d \leqslant r$ is the number of SRDMD modes used to reconstruct the velocity field. Following Page & Kerswell (2019), we set the coefficients c_j as those that minimise the cost function $\mathcal{J}(c_0, c_1, \ldots, c_{N_d-1}) = \sum_{k=0}^{m-1} \|\xi(t_k) - \tilde{\xi}(t_k)\|^2$, where $\| \ldots \|$ indicates the L_2 norm.

We compute the SVD of Ξ using the method of snapshots (Sirovich 1987b) and follow Holmes *et al.* (1996); Sirovich (1989) to truncate it such that a sufficiently large fraction c_σ of the total energy is captured and no neglected mode contains, on average, more than a small fraction c_χ of the energy contained in the first mode. Namely

$$\sum_{i=0}^{r-1} \sigma_i^2 > c_\sigma \sum_{i=0}^{m-1} \sigma_i^2 \quad \text{and} \quad \frac{1}{m-r} \sum_{i=r}^{m-1} \sigma_i^2 < c_\chi \sigma_0^2,$$ (4.2)

where σ_i are the singular values. For all of our results to follow, we set $c_\sigma = 99.99\%$ and $c_\chi = 0.1\%$ which we determined by ensuring that higher-rank truncations do not alter the leading SRDMD eigenvalues in the first two digits.

5. Locally-linear approximations by SRDMD

In the following, we demonstrate that the near-wall turbulence in channel flow can be transiently approximated by a linear modal expansion. To this end, we consider a turbulent channel flow simulation spanning a time interval $t \in [0, 2000]$ and compute SRDMD of the data sampled at $\delta t = 1$ over sliding time windows of length $T_w := m \delta t = 30, 60$, and 100. In order to compare different episodes and window lengths, we construct SRDMD approximations (4.1) with $N_d = 10$ (or 9, depending on the number of complex conjugate eigenvalues in the dominant part of the SRDMD spectra). We identify the dominant SRDMD modes by ordering them according to their normalised spectra (Tu *et al.* 2014) in descending
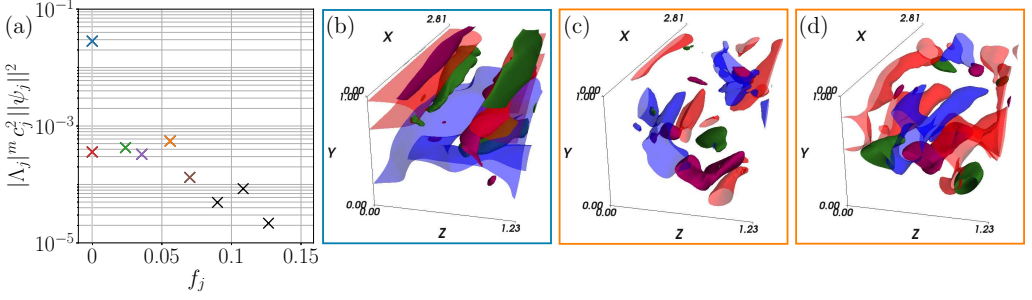
Figure 2: SRDMD in the time window $t \in [1280, 1340)$. (a) Normalised SRDMD spectrum where $f_j = |\mathrm{Im}\lambda_j|/2\pi$. The coloured symbols correspond to the modes that are included in the sum (4.1), while the black symbols are the first three discarded modes. (b–d) Three-dimensional visualizations of the SRDMD modes ψ_0 (b), $\mathrm{Re}\psi_1$ (c) and $\mathrm{Im}\psi_1$ (d).

$|\Lambda_j|^m c_j^2 \|\psi_j\|^2$ and keeping the leading N_d. Note that ordering the SRDMD modes in this way amplifies (penalizes) those that grow (decay) by multiplying them with their respective eigenvalue raised to m. As an example, fig. 2(a) shows the normalised SRDMD spectrum of a symmetry-reduced channel flow data window ($T_w = 60$), where the coloured crosses correspond to the dominant part of the spectrum and the black ones show the first three discarded modes. To illustrate the flow structures captured by SRDMD, fig. 2(b–d) shows three-dimensional visualizations of ψ_0, $\mathrm{Re}\psi_1$ and $\mathrm{Im}\psi_1$, respectively. In fig. 2(b–d) and the rest of the flow visualizations of this paper, the red/blue isosurfaces show $u = 0.5 \max/\min u$ and the green/purple isosurfaces show $\omega_x = 0.5 \max/\min \omega_x$, where ω_x is the streamwise vorticity.

We evaluate the accuracy of SRDMD by measuring the residual

$$\overline{\mathcal{R}}(t) = \frac{1}{m} \sum_{k=0}^{m-1} \frac{\|\tilde{\xi}(t + k\,\delta t) - \xi(t + k\,\delta t)\|}{\|\xi(t + k\,\delta t)\|}, \tag{5.1}$$

which is the mean relative error of the SRDMD approximation (4.1) to the time window $[t, t + T_w)$. Fig. 3 shows the residuals (5.1) of our SRDMD approximations with $N_d \leqslant 10$ to the sliding windows of the turbulent channel flow data. Low-error episodes are detected along the turbulent trajectory and appear to be clustered around certain time instants, for example around $t \approx 250, 950$ and 1250 (see fig. 3), thus signalling portions of the turbulent evolution that can be well captured by a reduced linear expansion. As expected, the dips in the $\overline{\mathcal{R}}(t)$ curve are most marked for the shortest window length $T_w = 30$, although they are still distinguishable for longer time windows, e.g. $T_w = 60$ or 100.

In the remainder of this section, we focus on the SRDMD approximations at $T_w = 60$, and illustrate the different dynamical behaviours captured by SRDMD via state space projections onto the dominant SRDMD modes. Fig. 4(a–c) show spiral-in (a) and out (b) dynamics as well as a nearly-periodic trajectory (c), along with their respective SRDMD approximations. We detected this nearly-periodic episode utilizing the periodicity indicator (Page & Kerswell 2020) $\varepsilon(n) := \frac{1}{n\omega_f^2} \sum_{j=1}^{n} |\mathrm{Im}\lambda_j - j\omega_f|^2$, where $\omega_f(n) := \frac{2}{n(n+1)} \sum_j^n \mathrm{Im}\lambda_j$ and the sums are carried over the n SRDMD eigenvalues with $\mathrm{Re}\lambda_j < \mu^{max}$ and $0 < \mathrm{Im}\lambda_1 < \ldots < \mathrm{Im}\lambda_{n-1} < \mathrm{Im}\lambda_n$. For an exactly periodic signal, $\varepsilon(n) = 0$ and its value below a threshold ε^{th} indicates approximate periodicity (Page & Kerswell 2020). The episode illustrated as a projection onto the plane spanned by the lowest-frequency SRDMD mode in fig. 4(c) was detected using $n = 4$, $\mu^{max} = 0.05$ and $\varepsilon^{th} = 10^{-3}$.
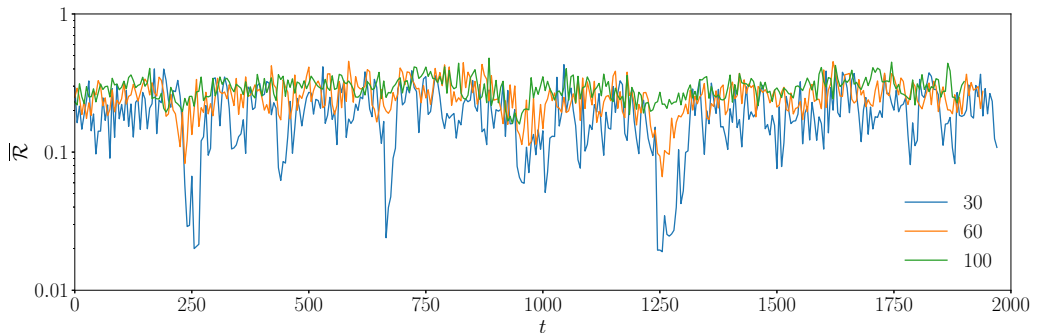
Figure 3: SRDMD residuals (5.1) for $T_w = 30, 60$, and 100.
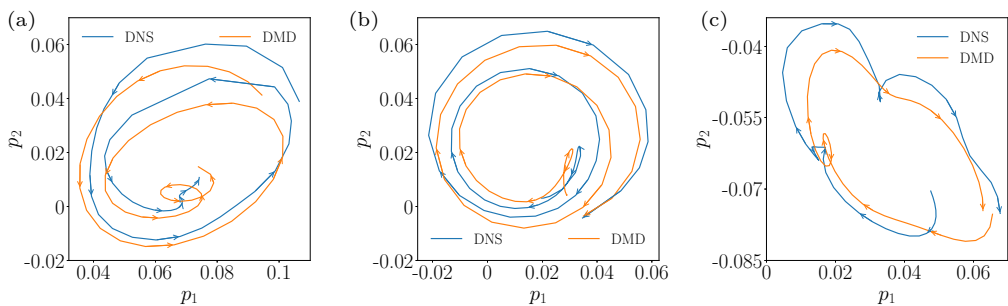
Figure 4: State-space projections corresponding to the time windows: (a) $t \in [265, 325)$, (b) $t \in [1280, 1340)$ and (c) $t \in [1295, 1355)$. The arrows indicate the direction of time. The projections are centred at the nearly neutral real mode ψ_0. The (p_1, p_2) planes correspond to those spanned by the leading (a, b) and lowest-frequency (c) complex conjugate SRDMD modes.

For the spiral-out event starting at $t = 1280$ (fig. 4(b)), we compare the evolution of the flow structures reconstructed using SRDMD to those of the original turbulent dynamics, see fig. 5 and Supplementary Movie 2. The SRDMD spectrum and the first two SRDMD eigenvectors were displayed in fig. 2. As shown in fig. 5, SRDMD can capture the evolution of streaks and rolls, visualised as isosurfaces of streamwise velocity and streamwise vorticity, respectively, with only 10 modes. In particular, it can capture the initial growth of the rolls which then break up into smaller structures and appear to decay towards the end of the time window while the streaks start meandering.

6. Necessity of symmetry reduction

In the previous section we demonstrated different dynamical regimes, such as spiral-in, spiral-out and nearly-periodic episodes that can be captured by SRDMD. We shall now show that a similar analysis without symmetry reduction yields DMD modes and associated eigenvalues that are completely dominated by the streamwise drifts. To this end, we compute here the standard DMD (without symmetry reduction) of the time window $t_s = [1280, 1340]$, where a spiralling-out behaviour was detected by the SRDMD. In contrast to the SRDMD spectrum (cf. fig. 2(a)), without symmetry reduction the spectrum shows a concentration of modes around the drift frequency $f_d = U_b/L_x \approx 0.23$, where $U_b = 2/3$ is the bulk velocity. Due to the fast advection in the streamwise direction, projections (not shown) onto one of these "drift modes" result in trajectories that show up as approximately circular dynamics. Furthermore,
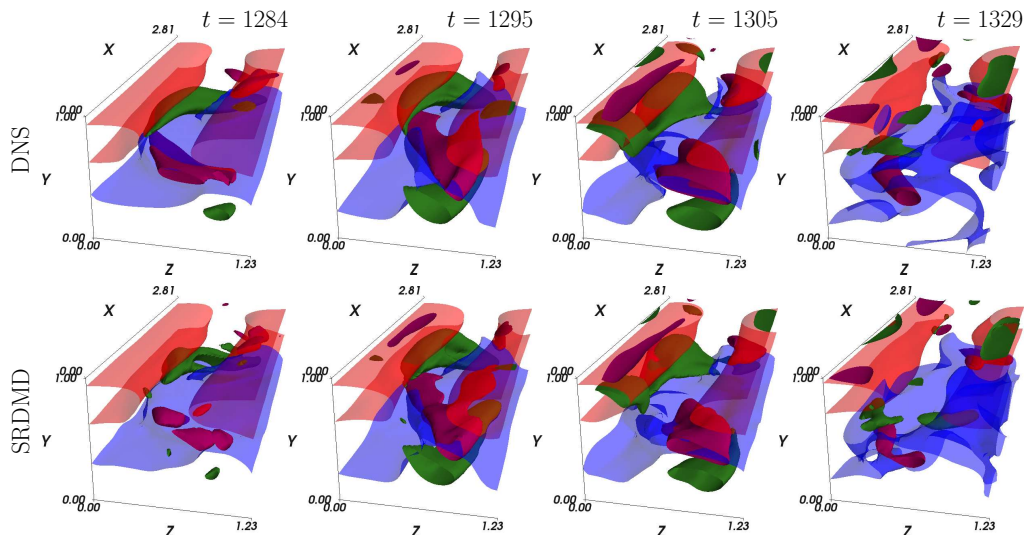
Figure 5: Three-dimensional visualizations of symmetry-reduced flow states and their SRDMD approximations for the time window $t \in [1280, 1340)$.
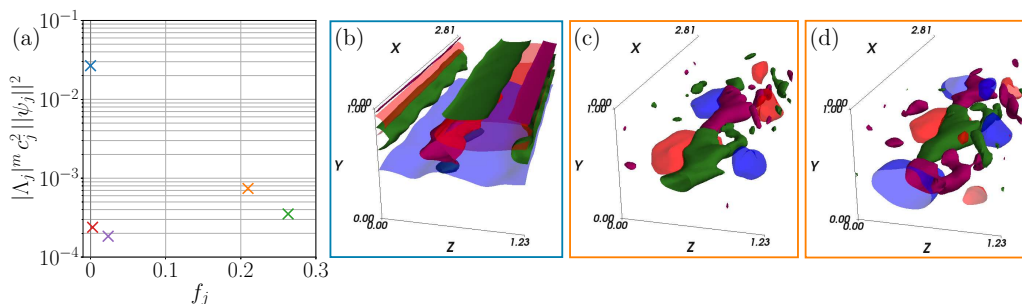
Figure 6: Standard DMD in the time window $t_s \in [1280, 1340)$ (to be compared with fig. 2). (a) Normalised DMD spectrum and three-dimensional visualisations of the eigenvectors ψ_0 (b), $\mathrm{Re}\psi_1$ (c) and $\mathrm{Im}\psi_1$ (d).

without symmetry reduction a temporal resolution $\delta t = 0.1$, ten times finer than that used in the symmetry-reduced case, was needed due to the clear separation between the time scales of the coherent structures and the advective units. While we can resolve the dynamics of coherent structures with a time step of $\delta t = 1$, the temporal resolution is completely lost if we do not eliminate the continuous symmetries. Finally, in contrast to the complex structures shown by SRDMD (cf. fig. 2(b–d)), the eigenvectors obtained from the standard DMD either just show elongated structures (fig. 6(b)), or align with the first streamwise Fourier mode (fig. 6(c, d)) as signified by the fact that $\mathrm{Im}\psi_1$ (fig. 6(d)) is virtually the same as $\mathrm{Re}\psi_1$ (fig. 6(c)) up to a quarter-domain shift in the x direction. This is further supported by the closeness of the associated temporal frequency $f_1 = 0.21$ to the drift frequency $f_d = 0.23$.

7. Conclusion and outlook

We have shown that low-dimensional behaviour in near-wall turbulence can be uncovered by the SRDMD of DNS data. As illustrated by our examples, SRDMD yields modal expansions that can transiently approximate turbulence, similar, in spirit, to the dynamics of a low-

Re flow in the vicinity of an ECS. In analogy to ECS, the episodes that we illustrated in §5 can be thought as those in the neighbourhoods of *pseudoequilibria* (fig. 4 (a, b)) and *pseudoperiodic* (fig. 4 (c)) solutions represented by SRDMD. A future research direction that we plan to explore is to use a finite set of *pseudoinvariant solutions* as bases of a coarse-grained turbulence model. Higher-dimensional pseudoinvariant solutions with multiple time scales, such as pseudoinvariant 2-tori, can be included in such a study by generalizing the periodicity indicator function of Page & Kerswell (2020) to higher dimensions. We, therefore, believe that the present study is a significant step towards extending deterministic approaches to turbulence towards high-*Re* flows with multiple time scales.

The symmetry reduction method presented here is easily applicable to other flows in rectangular domains, e.g. plane Couette or asymptotic boundary layer flows. While continuous symmetry reduction is a necessary preprocessing step for POD or DMD in these systems, we believe that nearly every dynamical study of such flows can benefit from eliminating the redundant data due to the symmetries. Thus, we recommend our symmetry reduction method for deterministic studies of fluid flows in channel geometries.

Author ORCID. E. Marensi, https://orcid.org/0000-0001-7173-4923; G. Yalnız, https://orcid.org/0000-0002-8490-9312; B. Hof, https://orcid.org/0000-0003-2057-2754; N. B. Budanur, https://orcid.org/0000-0003-0423-5010

REFERENCES

BUDANUR, N. B., BORRERO-ECHEVERRY, D. & CVITANOVIĆ, P. 2015a Periodic orbit analysis of a system with continuous symmetry – a tutorial. *Chaos* **25**, 073112, arXiv: 1411.3303.

BUDANUR, N. B., CVITANOVIĆ, P., DAVIDCHACK, R. L. & SIMINOS, E. 2015b Reduction of the SO(2) symmetry for spatially extended dynamical systems. *Phys. Rev. Lett.* **114**, 084102, arXiv: 1405.1096.

BUDANUR, N. B., DOGRA, A. S. & HOF, B. 2019 Geometry of transient chaos in streamwise-localized pipe flow turbulence. *Phys. Rev. Fluids* **4**, 102401, arXiv: 1810.02211.

BUDANUR, N. B. & HOF, B. 2017 Heteroclinic path to spatially localized chaos in pipe flow. *J. Fluid Mech.* **827, R1**, arXiv: 1703.10484.

BUDANUR, N. B. & HOF, B. 2018 Complexity of the laminar-turbulent boundary in pipe flow. *Phys. Rev. Fluids* **3**, 054401, arXiv: 1802.01918.

BUDANUR, N. B., SHORT, K. Y., FARAZMAND, M., WILLIS, A. P. & CVITANOVIĆ, P. 2017 Relative periodic orbits form the backbone of turbulent pipe flow. *J. Fluid Mech.* **833**, 274–301, arXiv: 1705.03720.

ECKHARDT, B., FAISST, H., SCHMIEGEL, A. & SCHNEIDER, T. M. 2008 Dynamical systems and the transition to turbulence in linearly stable shear flows. *Phil. Trans. R. Soc. A* **366** (1868), 1297–1315.

FARAZMAND, M. 2016 An adjoint-based approach for finding invariant solutions of Navier-Stokes equations. *J. Fluid Mech.* **795**, 278–312, arXiv: 1508.06363.

GIBSON, J. F., HALCROW, J. & CVITANOVIĆ, P. 2008 Visualizing the geometry of state space in plane Couette flow. *J. Fluid Mech.* **611**, 107–130, arXiv: 0705.3957.

GIBSON, J. F., REETZ, F., AZIMI, S., FERRARO, A., KREILOS, T., SCHROBSDORFF, H., FARANO, M., YESIL, A. F., SCHÜTZ, S. S., CULPO, M. & SCHNEIDER, T. M. 2020 Channelflow 2.0 (in preparation).

HAMILTON, J. M., KIM, J. & WALEFFE, F. 1995 Regeneration mechanisms of near-wall turbulence structures. *J. Fluid Mech.* **287**, 317–348.

HIRUTA, Y. & TOH, S. 2017 Intermittent direction reversals of moving spatially localized turbulence observed in two-dimensional Kolmogorov flow. *Phys. Rev. E* **96**, 063112, arXiv: 1706.04395.

HOLMES, P., LUMLEY, J. L. & BERKOOZ, G. 1996 *Turbulence, Coherent Structures, Dynamical Systems and Symmetry*. Cambridge: Cambridge Univ. Press.

JIMÉNEZ, J. 2018a Coherent structures in wall-bounded turbulence. *J. Fluid Mech.* **842**, P1, arXiv: 1710.07493.

JIMÉNEZ, J. 2018*b* Machine-aided turbulence theory. *J. Fluid Mech.* **854**, R1, arXiv: 1806.06247.

JIMÉNEZ, J. & MOIN, P. 1991 The minimal flow unit in near-wall turbulence. *J. Fluid Mech.* **225**, 213–240.

JIMÉNEZ, J. & PINELLI, A. 1999 The autonomous cycle of near-wall turbulence. *J. Fluid Mech* **389**, 335–359.

KAWAHARA, G., UHLMANN, M. & VAN VEEN, L. 2012 The significance of simple invariant solutions in turbulent flows. *Annu. Rev. Fluid Mech* **44**, 203–225, arXiv: 1108.0975.

KERSWELL, R. R. 2005 Recent progress in understanding the transition to turbulence in a pipe. *Nonlinearity* **18**, R17–R44.

KOOPMAN, B. O. 1931 Hamiltonian systems and transformations in Hilbert space. *Proc. Natl. Acad. Sci.* **17**, 315–318.

KUTZ, J. N., BRUNTON, S. L., BRUNTON, B. W. & PROCTOR, J. L. 2016 *Dynamic mode decomposition: data-driven modeling of complex systems*, , vol. 149. SIAM.

MENDIBLE, A., BRUNTON, S. L., ARAVKIN, A. Y., LOWRIE, W. & KUTZ, J. N. 2020 Dimensionality reduction and reduced-order modeling for traveling wave physics. *Theor. Comput. Fluid Dyn* **34** (4), 385–400.

MEZIĆ, IGOR 2005 Spectral properties of dynamical systems, model reduction and decompositions. *Nonlinear Dyn.* **41**, 309–325.

PAGE, J. & KERSWELL, R. 2019 Koopman mode expansions between simple invariant solutions. *J. Fluid Mech.* **879**, 1–27, arXiv: 1811.05907.

PAGE, J. & KERSWELL, R. R. 2020 Searching turbulence for periodic orbits with dynamic mode decomposition. *J. Fluid Mech.* **886**, A28, arXiv: 1906.01310.

POPE, S. B. 2000 *Turbulent Flows*. Cambridge: Cambridge Univ. Press.

ROWLEY, C. W. & DAWSON, S. T .M. 2017 Model reduction for flow analysis and control. *Ann. Rev. Fluid Mech.* **49**, 387–417.

ROWLEY, C. W. & MARSDEN, J. E. 2000 Reconstruction equations and the Karhunen-Loéve expansion for systems with symmetry. *Physica D* **142**, 1–19.

ROWLEY, C. W., MEZIĆ, I., BAGHERI, S., SCHLATTER, P. & HENNINGSON, D. S. 2009 Spectral analysis of nonlinear flows. *J. Fluid Mech.* **641**, 115.

SCHMID, P. & SESTERHENN, J. 2008 Dynamic mode decomposition of numerical and experimental data. In *61ˢᵗ Annual Meeting of the APS Division of Fluid Dynamics*, *Bull. Am. Phys. Soc*, vol. 61, pp. MR–007.

SCHMID, P. J. 2010 Dynamic mode decomposition of numerical and experimental data. *J. Fluid Mech.* **656**, 5–28.

SCHOPPA, W. & HUSSAIN, F. 2002 Coherent structure generation in near-wall turbulence. *J. Fluid Mech* **453**, 57–108.

SESTERHENN, J. & SHAHIRPOUR, A. 2019 A characteristic dynamic mode decomposition. *Theor. Comput. Fluid Dyn.* **33** (3-4), 281–305.

SIROVICH, L. 1987*a* Turbulence and the dynamics of coherent structures. ii. symmetries and transformations. *Quart. Appl. Math.* **45** (3), 573–582.

SIROVICH, L. 1987*b* Turbulence and the dynamics of coherent structures part I: coherent structures. *Quart. Appl. Math.* **45**, 561–571.

SIROVICH, L. 1989 Chaotic dynamics of coherent structures. *Physica D* **37** (1), 126 – 145.

SURI, B., TITHOF, J., GRIGORIEV, R. O. & SCHATZ, M. F. 2017 Forecasting fluid flows using the geometry of turbulence. *Phys. Rev. Lett.* **118**, 114501, arXiv: 1611.02226.

TU, J. H., ROWLEY, C. W., LUCHTENBURG, D. M., BRUNTON, S. L. & KUTZ, J. N. 2014 On dynamic mode decomposition: Theory and applications. *J. Comput. Dyn.* **1** (2), 391–421, arXiv: 1312.0041.

VAN VEEN, L. & KAWAHARA, G. 2011 Homoclinic tangle on the edge of shear turbulence. *Phys. Rev. Lett.* **107**, 114501.

WALEFFE, F. 1997 On a Self-Sustaining Process in shear flows. *Phys. Fluids* **9**, 883–900.

WALEFFE, F. 2001 Exact coherent structures in channel flow. *J. Fluid Mech.* **435**, 93–102.

WILLIS, A. P., SHORT, K. Y. & CVITANOVIĆ, P. 2016 Symmetry reduction in high dimensions, illustrated in a turbulent pipe. *Phys. Rev. E* **93**, 022204, arXiv: 1504.05825.